Development and Optimization of Estrogen-Loaded Chitosan Nanoparticles for Postmenopausal Hormone Replacement Therapy

Sharmila Deepak Kuskar[1,2*], Sapana Prabhakar Ahirrao[1]
[1]MET's Institute Of Pharmacy Bhujbal Knowledge City Adgaon, Nashik (M.S) 422 003 Maharashtra
[2] RSM's N N Sattha College of Pharmacy, Ahilyanagar, Maharashtra 414001
Corresponding Author*
Sharmila Deepak Kuskar
MET's Institute Of Pharmacy Bhujbal Knowledge City Adgaon, Nashik (M.S) 422 003 Maharashtra
sharmilakuskar1@gmail.com

ABSTRACT

The present study aimed to design, develop, and optimize estrogen-loaded chitosan nanoparticles for postmenopausal women to improve drug bioavailability, enhance encapsulation efficiency, and provide sustained drug release using the ionotropic gelation technique. Estrogen-loaded nanoparticles were prepared by ionotropic gelation using chitosan and sodium tripolyphosphate (STPP). A Box–Behnken design was employed to optimize the formulation variables, including chitosan concentration, STPP concentration, and magnetic stirring speed. The prepared formulations were evaluated for particle size, polydispersity index (PDI), zeta potential, drug content, entrapment efficiency, in vitro drug release, FTIR compatibility, and transmission electron microscopy (TEM). The optimized formulation (EF2) exhibited a particle size of 109.8 nm, PDI of 0.137, and zeta potential of −29.3 mV, indicating good stability. Drug content and entrapment efficiency were found to be 95.12% and 90.10%, respectively. In vitro release studies demonstrated sustained drug release with 95.42% cumulative drug release over 24 h. Response surface methodology confirmed the significant influence of formulation variables on particle size, drug content, and entrapment efficiency. Drug release kinetics followed the zero-order model ($R^2 = 0.9669$) and showed diffusion-controlled release behavior according to the Higuchi model ($R^2 = 0.9618$). FTIR studies confirmed the compatibility of the drug with formulation excipients. TEM analysis revealed predominantly spherical and well-dispersed nanoparticles with particle sizes ranging from 85 to 94 nm, confirming the nanoscale nature and uniform morphology of the optimized formulation. The developed estrogen-loaded chitosan nanoparticles successfully achieved high drug loading, excellent entrapment efficiency, nanosized particle distribution, uniform spherical morphology, and prolonged drug release. The optimized formulation EF2 demonstrated promising potential as an effective nanoparticulate delivery system for hormone replacement therapy in postmenopausal women, offering improved therapeutic efficacy, bioavailability, and patient compliance.

KEYWORDS
Estrogen; Chitosan nanoparticles; Postmenopausal women; Hormone replacement therapy; Ionotropic gelation; Box–Behnken design; Entrapment efficiency; Sustained drug release
How to cite this article: Kuskar SD, Ahirrao SP. Development and Optimization of Estrogen-Loaded Chitosan Nanoparticles for Postmenopausal Hormone Replacement Therapy. Int J Drug Deliv Technol. 2026;16(69s): 1648-1657. DOI: 10.25258/ijddt.16.69s.160

1. INTRODUCTION

Menopause is a natural physiological transition that generally occurs between 48 and 55 years of age in Indian women, although early menopause may occur between 45–50 years and premature menopause before 40 years. Owing to increased life expectancy, women spend nearly one-third of their lives in the postmenopausal stage, making postmenopausal health a major public health concern worldwide [1,2]. Estrogen deficiency following menopause is associated with numerous physiological and psychological complications, including cardiovascular diseases, osteoporosis, osteoarthritis, urogenital disorders, obesity, cognitive decline, depression, and an increased risk of certain cancers [3–5]. These complications significantly reduce the quality of life of ageing women and contribute to increased morbidity and healthcare burden [6-9].

Hormone Replacement Therapy (HRT) remains one of the most effective approaches for managing menopausal symptoms and preventing long-term complications associated with estrogen deficiency [10-12]. However, conventional hormone therapy is often limited by poor bioavailability, extensive first-

pass metabolism, frequent dosing requirements, systemic adverse effects, and poor patient compliance [13-14]. Therefore, the development of advanced drug delivery systems capable of improving therapeutic efficacy while minimizing side effects has become an important area of pharmaceutical research [15].

Nanoparticle-based drug delivery systems have emerged as promising carriers for hormone delivery due to their ability to enhance drug solubility, stability, permeability, and bioavailability [12,13]. Nanoparticle formulations can improve the absorption of poorly water-soluble drugs by increasing dissolution rates and facilitating transcellular and paracellular transport across biological membranes [14,15]. The physicochemical characteristics of nanoparticles, including particle size, surface morphology, and chemical composition, significantly influence drug absorption, distribution, and elimination [16]. Nanometer-sized particles provide a larger surface area, resulting in enhanced dissolution, improved permeability, and superior therapeutic performance compared with conventional formulations [17].

Furthermore, nanoparticle carriers offer controlled and sustained drug release, protection of hormones from enzymatic degradation, targeted delivery, and reduced systemic toxicity [18,19]. Several studies have demonstrated that polymeric and lipid-based nanoparticles can effectively improve the pharmacokinetic and pharmacodynamic profiles of therapeutic agents while reducing dose-related adverse effects [20]. These advantages make nanoparticle-mediated hormonal therapy an attractive strategy for addressing the challenges associated with conventional hormone replacement therapy in postmenopausal women.

Estrogen-loaded nanoparticles have the potential to provide sustained hormone release, improve bioavailability, reduce dosing frequency, and enhance therapeutic efficacy while minimizing systemic side effects. Such advanced delivery systems may contribute to the prevention and management of menopause-associated disorders, including osteoporosis, cardiovascular diseases, and urogenital complications. Therefore, the design and development of nanoparticle-based hormonal formulations represent a promising approach for improving postmenopausal healthcare and enhancing the overall quality of life of ageing women.

2. MATERIALS AND METHODS

2.1 Materials

Estrogen was procured from Solanki Enterprises, Pune. STPP (Sodium tripolyphosphate), chitosan, acetic acid was procured from Research Lab Fine Chem Industries Pvt. Ltd., Mumbai, India. All chemicals and excipients used in the study were of analytical grade.

2.2 Methods

2.2.1 Formulation and evaluation of nanopartcle

Method: Ionotropic Gelation Method

0.25% W/V STPP (Sodium tripolyphosphate) solution was prepared containing pH 7-9. Adjust pH by using 2 M NaOH solution. Chitosan with various concentrations was dissolved in aqueous solution of acetic acid (1% V/V) on magnetic stirrer at 500 rpm. Adjust pH up to 4-6. After the complete dissolution of chitosan, the drugs were added in to the above solution and again stirrer at 500 rpm on magnetic stirrer. The above drug and chitosan solution was sonicated for 15 min on ultra-sonicate. The alkaline STPP solution was added drop wise in to the acidic solution of chitosan containing drugs molecules. Then there is formation of chitosan drug loaded nanoparticle [21,22].

Experimental design

The response surface methodology (RSM) was employed to perform Quality by Design approach for constructing and investigating the polynomial models, using fewer experimental runs. Box-Behnken Design comprising of 3-factors and 3- levels was employed to examine the quadratic response surfaces by assessing the effect of pre-defined independent variables on different response dependent variables Drug content (%), Particle Size (nm) and Entrapment Efficiency (%) was coded as Y1, Y2 and Y3. Three independent variables namely Chitosan (mg) (A), STPP (%) (B) and Homogenization Speed (C) (rpm) were chosen. Each of the variables was varied at two different levels, known as high, and low levels. All the finalized independent variables and the response variables are described in Table 1

Table 1: List of Independent and Dependent variables in Box–Behnken design

Independent variables	**Low value(-1)**	**Medium (0)**	**High value(+)**
Chitosan (mg) (A)	10	30	50
STPP (%) (B)	0.5	0.75	1
magnetic Stirrer (RPM) (C)	1500	1750	2000
Dependent variables	Constraints		
Drug Content (%)	Maximize		
Particle Size (nm)	Minimize		

Entrapment efficiency (%)	Maximize		

Table 2: DOE Suggested and Experimental batches

Formulation code	Estrogen (mg)	Chitosan (mg)	STPP (%)	STPP (ml)	Magnetic Stirrer (RPM)	Acetic acid (ml)	Lactobacillus (ml)
EF1	13.75	10	0.75	2	1500	10	1
EF2	13.75	30	0.75	2	1750	10	1
EF3	13.75	10	0.75	2	2000	10	1
EF4	13.75	50	0.5	2	1750	10	1
EF5	13.75	50	1	2	1750	10	1
EF6	13.75	10	1	2	1750	10	1
EF7	13.75	50	0.75	2	2000	10	1
EF8	13.75	50	0.75	2	1500	10	1
EF9	13.75	30	0.5	2	1500	10	1
EF10	13.75	30	1	2	1500	10	1
EF11	13.75	30	0.5	2	2000	10	1
EF12	13.75	30	1	2	2000	10	1
EF13	13.75	10	0.5	2	1750	10	1

3. Evaluation of nanoparticle

3.1 Measurement of particle size, polydispersity index and zeta potential

The particle size of nanoparticle was determined by using dynamic light scattering (DLS) HORIBA (SZ-100V2) with a scattering angle of 90° at 25°C. The particle size analysis data obtained were evaluated using the intensity profile. The formed nanoparticle were suitably diluted (1:10) with milli-Q water before analysis [23].

3.2 Total drug content

Drug content was determined to assess the uniformity and efficiency of drug incorporation in the prepared formulation. An accurately weighed amount of the sample (equivalent to a known amount of drug) was dissolved in a simulated vaginal fluid pH 4.5 to ensure complete extraction of the drug. The solution was then filtered or centrifuged to remove any undissolved particles. The clear filtrate was analyzed using a UV–Visible spectrophotometer (Jasco V- 630) at the 271 nm. The drug content (%) was calculated using the following formula [24]:

Drug Content (%) = Measured drug concentration/ Theoretical drug concentration *100

3.3 Entrapment efficiency (EE)

Encapsulation efficiency (EE) was determined to evaluate the percentage of drug successfully entrapped within the formulation. A known amount of the prepared formulation was dispersed in simulated vaginal fluid pH 4.5 and then centrifuged (Eltek Model no. OC 2F) to separate the free (unencapsulated) drug in the supernatant. The amount of free drug was quantified using a UV–Visible spectrophotometer (Jasco V-630) at 271 nm. The encapsulation efficiency was then calculated using the formula [24]:

Encapsulation Efficiency (%) = Total drug−Free drug / Total drug *100

3.4 In-vitro diffusion studies

The modified Franz diffusion cell at 37°C which is fitted with a dialysis membrane having a molecular weight cut off 350 Da was used for study. The membrane was soaked in boiling distilled water for 12 hours before mounting to Franz diffusion cell. dispersion 2 ml was placed in to the donor compartment and the 20 ml of phosphate buffer 4.5 is used to fill receptor compartment. With different time interval of 2, 4, 6, 8, 12, 24 hrs 5 ml of sample was withdrawn and analysed using UV spectrophotometer (Jasco V-630) at 271 nm. Sink conditions were maintained in the receptor compartment during in-vitro release studies. The experiment was carried out in triplicate (n-3) [25].

3.5 FTIR

FTIR spectra were recorded using the FT/IR-4600 Type A (Model No. F193061786) equipped with an ATR accessory. A small amount of nanoparticle was placed directly onto the ATR crystal and pressed with the pressure arm. Spectra were collected from 4000–400 cm^{-1} with a resolution of 4 cm^{-1} and 32 scans, using a background spectrum recorded before each measurement. The spectra were baseline corrected and normalized for comparison [26].

3.6 Transmission Electron Microscopy (TEM) (JEOL, 2200FS)

TEM is done for analysis of surface morphology. Transmission Electron Microscopy (TEM) The surface morphology of the optimized batch EF2 was established by using Transmission Electron Microscopy (TEM). Few microliters of diluted nanoparticle solution of optimized batch FE2 was put on 300 mesh copper grid film coated with copper and were air-dried at room temperature. Once it was dried

completely, the sample was stained using a 2 %w/v phosphotungstic acid solution removing the excess with a filter paper. Further, the analysis and images of samples were captured by using digital micrograph and Soft Imaging Viewer Software [27].

4. RESULTS AND DISCUSSION

4.1 Particle size and zeta potential

Table 3: Particle size and zeta potential of EF1 to EF13

Formulation Code	Particle size (nm)	PDI	Zeta potential (mV)
EF1	123.4	0.136	-21.9
EF2	**109.8**	**0.137**	**-29.3**
EF3	115.1	0.131	-18.6
EF4	138.9	0.133	-26.3
EF5	139.1	0.134	-23.4
EF6	132.7	0.138	-21.4
EF7	125.4	0.139	-28.2
EF8	120.2	0.144	-19.7
EF9	128.3	0.123	-20.8
EF10	133.2	0.116	-25.3
EF11	128.3	0.138	-26.6
EF12	126.3	0.125	-23.7
EF13	129.7	0.138	-27.2

The particle size of the nanoparticle formulations ranged from 109.8 to 139.1 nm, PDI ranged from 0.116 to 0.144, and zeta potential ranged from −18.6 to −29.3 mV. The results indicated a narrow particle size distribution and good physical stability, confirming the successful formation of nanoparticles.

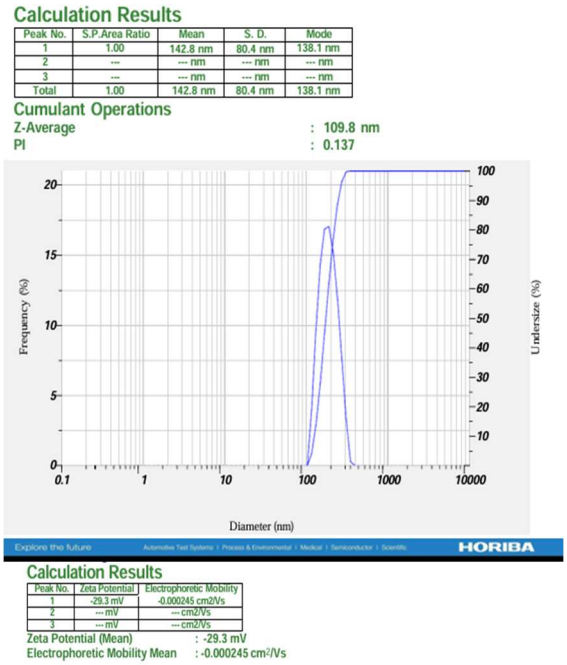

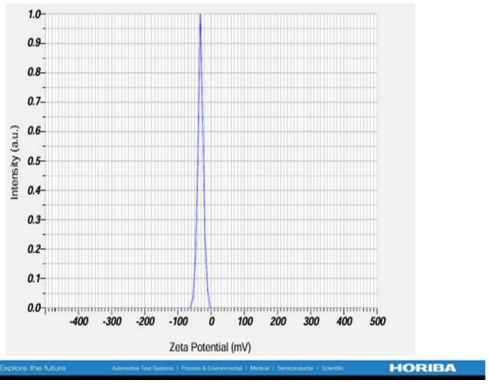

Fig 1: Particle size of EF2 **Fig 2: Zeta potential of EF2**

ANOVA for Quadratic model

Response 2: Particle Size

$Y=109.80+2.84A+0.7625B-1.25C-0.70AB+3.38AC-1.72BC+8.65A2+16.65B2+2.57C2$

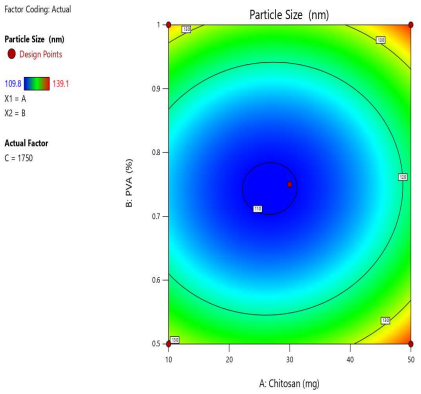

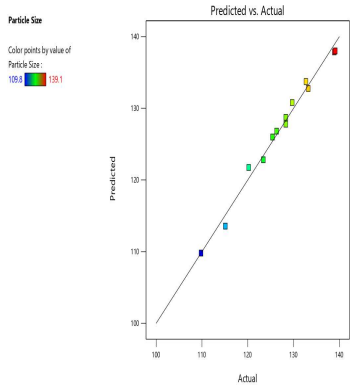

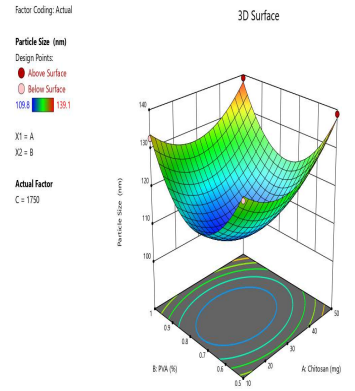

A) **B)**

C)

Fig 3 A: Counter plot, Fig 4B: Predicted vs Actual plot, Fig 5C: 3D Surface plot

4.2 Drug content

Table 4: Drug content of EF1 to EF13

Formulation Code	Drug content (%)
EF1	90.18 ± 0.0001
EF2	**95.12 ± 0.0001**
EF3	90.43 ± 0.0001
EF4	87.56 ± 0.0002
EF5	84.4 ± 0.0001
EF6	92.2 ± 0.0002
EF7	90.76 ± 0.0001
EF8	86.69 ± 0.0001
EF9	91.25 ± 0.0009
EF10	83.2 ± 0.0001
EF11	82.6 ± 0.0001
EF12	92.8 ± 0.0001
EF13	86.52 ± 0.0001

The drug content of formulations EF1–EF13 ranged from 82.60 ± 0.0001% to 95.12 ± 0.0001%. Among all formulations, EF2 showed the highest drug content (95.12 ± 0.0001%) and was selected as the optimized batch due to its superior drug loading and uniform drug distribution. The results indicate efficient drug incorporation in the developed nanoparticle formulations.

ANOVA for Quadratic model

Response 1: Drug Content

Drug Content (%)=95.12−1.24A+0.5837B+0.6587C−2.21AB+0.9550AC+4.56BC−2.70A2−4.75B2−2.91C2

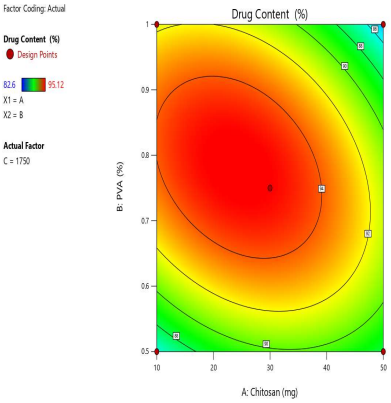

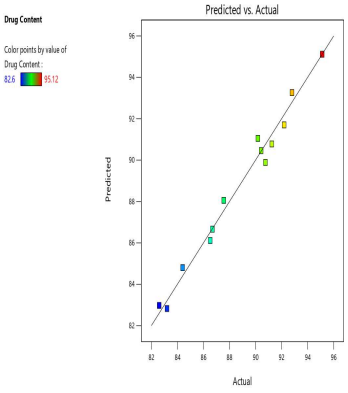

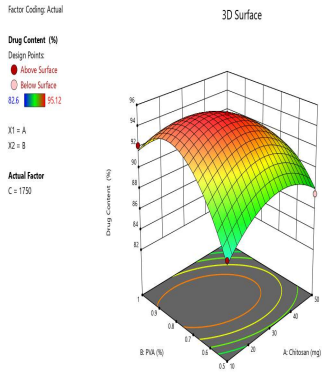

A) **B)**

C)

Fig 6A: Counter plot, Fig 7B: Predicted vs Actual plot, Fig 8C: 3D Surface plot

4.3 Encapsulation Efficiency

Table 5: Encapsulation Efficiency of EF1 to EF13

Formulation Code	Encapsulation Efficiency (%)
EF1	88.07 ± 0.0011
EF2	**90.10 ± 0.0017**
EF3	75.52 ± 0.0009
EF4	79.45 ± 0.0024
EF5	82.25 ± 0.0024
EF6	86.61 ± 0.0018
EF7	79.51 ± 0.0038
EF8	72.65 ± 0.0041
EF9	71.2 ± 0.0022
EF10	81.8 ± 0.0024
EF11	74.18 ± 0.0029
EF12	76.62 ± 0.0032
EF13	77.6 ± 0.0030

The encapsulation efficiency of formulations EF1–EF13 showed noticeable variation, reflecting the influence of formulation variables. EF2 exhibited the highest encapsulation efficiency (90.10%), followed by EF1 and EF6, indicating effective drug entrapment. Lower encapsulation efficiencies were observed in EF8 and EF9, though all formulations demonstrated reasonable drug loading. Overall, the results confirm that the formulation approach is capable of achieving satisfactory encapsulation efficiency, with EF2 emerging as the most promising formulation.

ANOVA for Quadratic model

Response 3: Entrapment efficiency

Entrapment Efficiency (%)=90.10−1.99A+3.36B−0.9862C−2.05AB+4.85AC−2.04BC−2.57A2−5.55B2−8.60C2

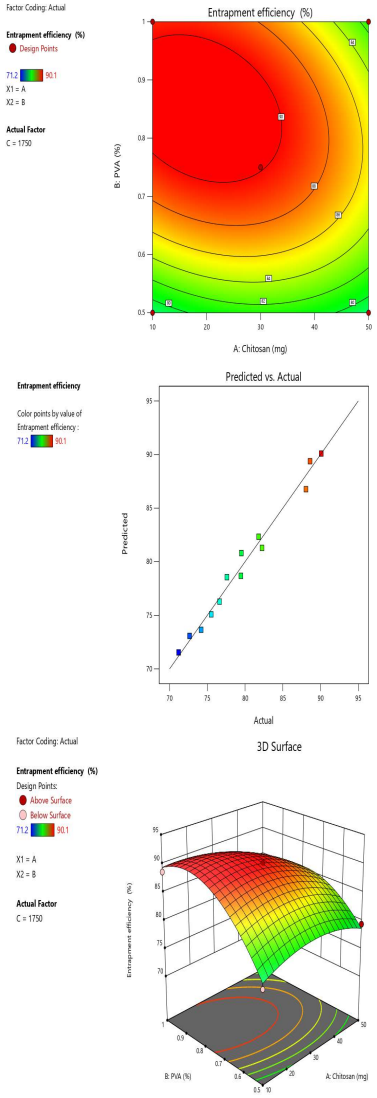

A) **B)**

C)

Fig 9A: Counter plot, Fig 10B: Predicted vs Actual plot, Fig 11C: 3D Surface plot

4.4 In-vitro diffusion studies

Table 6: In vitro Drug Release of EF1 to EF6

Time (Hr)	EF1	EF2	EF3	EF4	EF5	EF6
0	0	0	0	0	0	0
2	11.97 ± 0.0021	12.51 ± 0.0051	11.57 ± 0.0004	10.47 ± 0.0008	9.87 ± 0.0058	8.52 ± 0.0005
4	22.8	24.58 ±	20.07 ±	19.10 ±	18.60 ±	17.75 ±

	5 ± 0.00036	0.0047	0.0069	0.0074	0.0040	0.0057
6	33.80 ± 0.00058	36.80 ± 0.0091	31.78 ± 0.0041	30.80 ± 0.0081	29.08 ± 0.0002	27.89 ± 0.0014
8	43.76 ± 0.01001	46.98 ± 0.0071	41.31 ± 0.0008	38.76 ± 0.0093	37.71 ± 0.0041	36.10 ± 0.0081
12	55.62 ± 0.0369	59.05 ± 0.0002	51.75 ± 0.0091	48.62 ± 0.0038	45.75 ± 0.0017	42.89 ± 0.0007
24	94.00 ± 0.1274	95.42 ± 0.0058	91.03 ± 0.0005	89.95 ± 0.0048	87.03 ± 0.0058	83.07 ± 0.0008

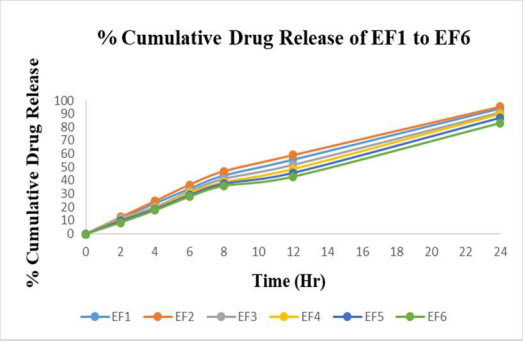

Fig 12: In vitro Drug Release of EF1 to EF6

Table 7: In vitro Drug Release of EF7 to EF13

Time (Hr)	EF 7	EF 8	EF 9	EF 10	EF 11	EF 12	EF 13
0	0	0	0	0	0	0	0
2	11.92	10.91	9.998	9.627	9.464	8.89 ± 0.068	8.582 ± 0.296
4	23.95 ± 0.025	22.75 ± 0.357	21.02 ± 0.000	19.45 ± 0.048	17.89 ± 0.147	17.02 ± 0.741	16.74 ± 0.674
6	34.64 ± 0.000	32.63 ± 0.147	30.93 ± 0.143	29.64 ± 0.014	28.92 ± 0.578	27.93 ± 0.648	26.23 ± 0.347
8	44.99 ± 0.025	43.02 ± 0.624	41.98 ± 0.357	39.99 ± 0.037	38.56 ± 0.678	36.92 ± 0.982	35.88 ± 0.178
12	57.6 ± 0.068	55.04 ± 0.025	53.89 ± 0.258	51.6 ± 0.068	49.04 ± 0.697	47.50 ± 0.007	45.05 ± 0.674
24	93.78 ± 0.347	91.29 ± 0.000	89.95 ± 0.014	87.98 ± 0.037	85.08 ± 0.012	84.4 ± 0.025	83.6 ± 0.640

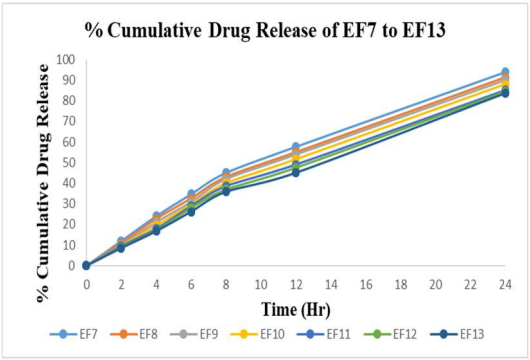

Fig 13: In vitro Drug Release of EF7 to EF13

The in vitro drug release profiles of formulations EF1–EF13 showed a time-dependent and sustained release pattern over 24 hours. Among all formulations, EF2 exhibited the highest cumulative drug release (96.73%), followed closely by EF1 and EF7, indicating superior release characteristics. Formulations EF3–EF6 and EF8–EF13 demonstrated comparatively slower release, with EF6 and EF13 showing the lowest cumulative release at 24 hours. Overall, the results confirm that formulation variables significantly influenced drug release behavior, with EF2 emerging as the most optimized formulation for prolonged and efficient drug release.

Kinetic analysis of drug release-

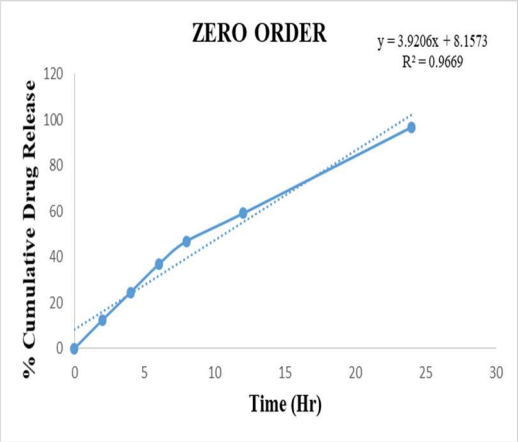

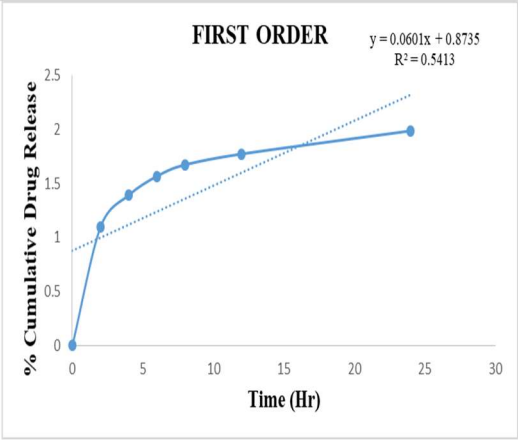

Fig 14: Zero order model of EF2 **Fig 15: First order model of EF2**

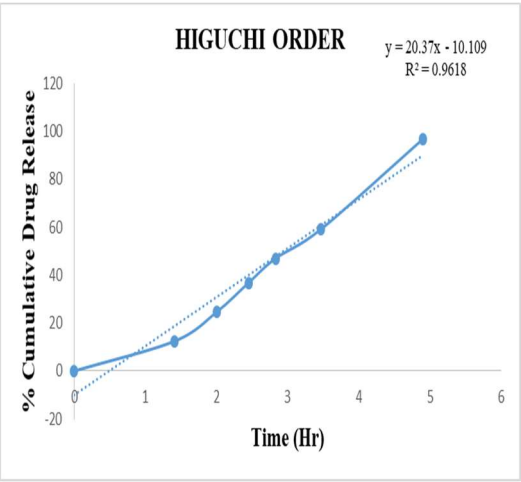

Fig 16: Higuchi model of EF2

The in vitro drug release data of the optimized formulation EF2 were fitted into various kinetic models to determine the mechanism of drug release. Among the tested models, the Zero-order model exhibited the highest correlation coefficient (R^2 = 0.9669), followed by the Higuchi model (R^2 = 0.9618), whereas the First-order model showed a comparatively lower R^2 value (0.5413). The higher R^2 value obtained for the zero-order model indicates that the drug release from EF2 followed a concentration-independent and controlled release pattern. The good fit to the Higuchi model further suggests that the drug release occurred predominantly through a diffusion-controlled mechanism. Therefore, it can be concluded that the optimized nanoparticle formulation EF2 provided sustained and controlled drug release, making it a promising carrier system for prolonged therapeutic action.

4.5 FTIR

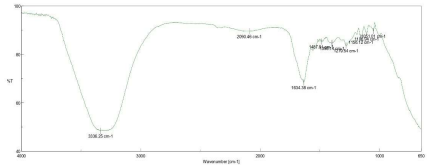

Fig 17: FTIR of optimized batch EF2

Table 8: FTIR of optimized batch EF2

Wavenumber (cm^{-1})	Functional Group
~3300–3350	O–H stretching
~2900	C–H stretching
~1650	C=O stretching (Amide I)
~1540–1560	N–H bending, C–N stretching (Amide II)
~1400–1450	C–H bending
~1000–1150	C–O–C stretching

The FTIR spectrum exhibited all the characteristic peaks of chitosan and PVA, confirming the presence and integrity of the polymeric components in the formulation. The broad O–H stretching band around 3300–3350 cm^{-1} indicated strong hydrogen bonding within the polymer matrix. The peaks observed at ~1650 cm^{-1} (amide I) and 1540–1560 cm^{-1} (amide II) confirmed the presence of amide functional groups characteristic of chitosan. Additionally, the C–H stretching and bending vibrations reflected the stability of the polymer chains. The strong C–O–C stretching band further confirmed the polysaccharide backbone, indicating successful formulation without any chemical incompatibility.

4.6 TEM

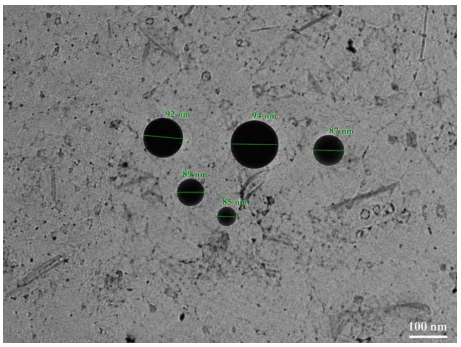

Fig 18: TEM of optimized batch EF2

The TEM image of the optimized batch EF2 revealed that the nanoparticles were predominantly spherical in shape with a relatively uniform size distribution. The particle sizes measured from the TEM micrograph ranged from 85 to 94 nm, confirming the formation of nanoparticles within the nanometric range. The particles appeared discrete and well-dispersed with minimal aggregation, indicating good formulation stability. The observed particle size was consistent with the nano-sized characteristics expected for the optimized formulation and supports the enhanced surface area and potential improvement in dissolution and bioavailability. Overall, the TEM study confirmed the successful preparation of uniformly distributed spherical nanoparticles in the optimized batch EF2.

5. CONCLUSION

The present study successfully developed and optimized estrogen-loaded chitosan nanoparticles for potential application in postmenopausal hormone replacement therapy. Nanoparticles were prepared using the ionotropic gelation method and optimized through a Box–Behnken experimental design. The formulation variables significantly influenced particle size, drug content, and entrapment efficiency. Among all formulations, EF2 was identified as the optimized batch, exhibiting a particle size of 109.8 nm, zeta potential of −29.3 mV, drug content of 95.12%, and entrapment efficiency of 90.10%.

The optimized nanoparticles demonstrated a narrow size distribution, good physical stability, and efficient drug incorporation. In vitro drug release studies revealed sustained and controlled release of estrogen over 24 hours, with cumulative drug release exceeding 95%. Drug release kinetic analysis indicated that the release followed a zero-order model with diffusion-controlled characteristics. FTIR analysis confirmed the compatibility of estrogen with formulation excipients and indicated the absence of significant drug–polymer interactions.

Transmission Electron Microscopy (TEM) analysis further confirmed the successful formation of nanoparticles with a predominantly spherical morphology and smooth surface characteristics. The particle size observed by TEM ranged from 85 to 94 nm, indicating a relatively uniform size distribution and minimal particle aggregation. The nanosized particles were well dispersed, supporting the findings obtained from particle size analysis and demonstrating the stability and homogeneity of the optimized formulation.

Overall, the developed estrogen-loaded chitosan nanoparticles showed favorable physicochemical properties, high encapsulation efficiency, uniform spherical morphology, and prolonged drug release behavior. These findings suggest that the optimized nanoparticle system may serve as a promising carrier for estrogen delivery, potentially improving bioavailability, therapeutic efficacy, and patient compliance in postmenopausal women. Further in vivo and clinical investigations are warranted to establish its safety, effectiveness, and long-term therapeutic potential.

6. CONFLICT OF INTEREST

The authors declare that they have no conflict of interest.

7. REFERENCES

1. Singh A, Pradhan SK. Menopausal symptoms of postmenopausal women in a rural community of Delhi, India: A cross-sectional study. Journal of mid-life health. 2014 Apr 1;5(2):62-7.
2. Mahajan N, Aggarwal M, Bagga A. Health issues of menopausal women in North India. Journal of mid-life Health. 2012 Jul 1;3(2):84-7.
3. Sukul S, Ghosh D. Studies on coronary heart disease (CHD) risk between reproductive age group and post-menopausal age group female population of Bankura district of West Bengal, India. IJHSR. 2016;6(12):83-90.
4. Bulliyya G. Risk of coronary heart disease in women after menopause. JOURNAL-INDIAN MEDICAL ASSOCIATION. 2001 Sep 1;99(9):478-82.
5. Christian RC, Harrington S, Edwards WD, Oberg AL, Fitzpatrick LA. Estrogen status correlates with the calcium content of coronary atherosclerotic plaques in women. The Journal of Clinical Endocrinology & Metabolism. 2002 Mar 1;87(3):1062-7.
6. Roman-Blas JA, Castañeda S, Largo R, Herrero-Beaumont G. Osteoarthritis associated with estrogen deficiency. Arthritis research & therapy. 2009 Sep 21;11(5):241.
7. Høegh-Andersen P, Tankó LB, Andersen TL, Lundberg CV, Mo JA, Heegaard AM, Delaissé JM, Christgau S. Ovariectomized rats as a model of postmenopausal osteoarthritis: validation and application. Arthritis Res Ther. 2004 Feb 19;6(2):R169.
8. Ham KD, Oegema TR, Loeser RF, Carlson CS. Effects of long-term estrogen replacement therapy on articular cartilage IGFBP-2, IGFBP-3, collagen and proteoglycan levels in ovariectomized cynomolgus monkeys. Osteoarthritis and cartilage. 2004 Feb 1;12(2):160-8.
9. Oskay UY, Beji NK, Yalcin O. A study on urogenital complaints of postmenopausal women

aged 50 and over. Acta obstetricia et gynecologica Scandinavica. 2005 Jan 1;84(1):72-8.

10. Amrita S, Pradeep P, Kakoli G, Sudip B, Naresh M, Sudha Y, Dipesh P. A study on health profile of post-menopausal women in Jamnagar district, Gujarat. Journal of research in medical and dental science. 2014 Apr;2(2):25.
11. Soares CD, Cohen LS. The perimenopause, depressive disorders, and hormonal variability. Sao Paulo Medical Journal. 2001 Mar 19;119(2):78-83.
12. Ghosh D, Singha PS, Parida P. Postmenopausal health of Indian women: A review. Current Women's Health Reviews. 2019 Feb 1;15(1):64-9.
13. Prakash IJ, Murthy VN. Psychiatric morbidity and the menopause. Indian journal of psychiatry. 1981 Jul 1;23(3):242-6.
14. Fernandez E, Gallus S, Bosetti C, Franceschi S, Negri E, La Vecchia C. Hormone replacement therapy and cancer risk: a systematic analysis from a network of case-control studies. International journal of cancer. 2003 Jun 20;105(3):408-12.
15. We JS, Han K, Kwon HS, Kil K. Effect of maternal age at childbirth on obesity in postmenopausal women: a nationwide population-based study in Korea. Medicine. 2016 May 1;95(19):e3584.
16. Li SD, Huang L. Pharmacokinetics and biodistribution of nanoparticles. Molecular pharmaceutics. 2008 Aug 4;5(4):496-504.
17. Lee JI, Nguyen VT, Chen ML, Adamson PC. A rapid, sensitive and selective liquid chromatography/atmospheric pressure chemical ionization tandem mass spectrometry method for determination of fenretinide (4-HPR) in plasma. Journal of Chromatography B. 2008 Feb 1;862(1-2):64-71.
18. Mainardes RM, Evangelista RC. PLGA nanoparticles containing praziquantel: effect of formulation variables on size distribution. International journal of pharmaceutics. 2005 Feb 16;290(1-2):137-44.
19. Martinez MN, Amidon GL. A mechanistic approach to understanding the factors affecting drug absorption: a review of fundamentals. The Journal of Clinical Pharmacology. 2002 Jun;42(6):620-43.
20. Mata NL, Lichter JB, Vogel R, Han Y, Bui TV, Singerman LJ. Investigation of oral fenretinide for treatment of geographic atrophy in age-related macular degeneration. Retina. 2013 Mar 1;33(3):498-507.
21. Das S, Banerjee R, Bellare J. Aspirin loaded albumin nanoparticles by coacervation: implications in drug delivery. Trends in Biomaterials and Artificial Organs. 2005 Jan 1;18(2):203-13. PS
22. Abdel-Nasser A, Fathy HM, Badr AN, Barakat OS, Hathout AS. Chitosan nanoparticles loaded with Lactobacillus rhamnosus bioactive metabolites: Preparation, characterization, and antifungal activity. Heliyon. 2025 Jan 30;11(2).
23. Sheu TY, Marshall RT. Microentrapment of lactobacilli in calcium alginate gels. Journal of food science. 1993 May;58(3):557-61.
24. Nesalin JA, Smith AA. Preparation and evaluation of stavudine loaded chitosan nanoparticles. Journal of Pharmacy Research. 2013 Feb 1;6(2):268-74.
25. Turanlı Y, Acartürk F. Preparation and characterization of colon-targeted pH/Time-dependent nanoparticles using anionic and cationic polymethacrylate polymers. European Journal of Pharmaceutical Sciences. 2022 Apr 1;171:106122.
26. Chauhan I, Yasir M, Verma M, Singh AP. Nanostructured lipid carriers: A groundbreaking approach for transdermal drug delivery. Advanced pharmaceutical bulletin. 2020 Feb 18; 10(2):150.
27. Kaul S, Jain N, Pandey J, Nagaich U. Investigating the retention potential of chitosan nanoparticulate gel: Design, development, in vitro & ex vivo characterization. Recent Patents on Anti-Infective Drug Discovery. 2020 Apr 1;15(1):41-67.